

# PCCP

Accepted Manuscript

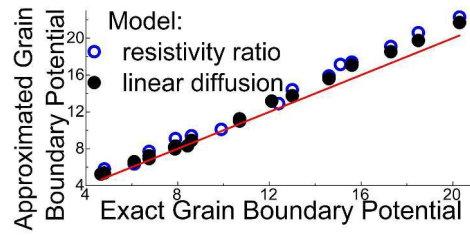


This is an *Accepted Manuscript*, which has been through the Royal Society of Chemistry peer review process and has been accepted for publication.

*Accepted Manuscripts* are published online shortly after acceptance, before technical editing, formatting and proof reading. Using this free service, authors can make their results available to the community, in citable form, before we publish the edited article. We will replace this *Accepted Manuscript* with the edited and formatted *Advance Article* as soon as it is available.

You can find more information about *Accepted Manuscripts* in the [Information for Authors](#).

Please note that technical editing may introduce minor changes to the text and/or graphics, which may alter content. The journal's standard [Terms & Conditions](#) and the [Ethical guidelines](#) still apply. In no event shall the Royal Society of Chemistry be held responsible for any errors or omissions in this *Accepted Manuscript* or any consequences arising from the use of any information it contains.



Combining the linear diffusion and the resistivity ratio models, one can distinguish between the grain boundary resistance related to space charge from the resistance from other sources

**On determining the height of the potential barrier at grain boundaries in ion-conducting oxides**Sangtae Kim\*<sup>1</sup>, Seong K. Kim<sup>1</sup>, Sergey Khodorov<sup>2</sup>, Joachim Maier<sup>3</sup> and Igor Lubomirsky\*<sup>2</sup><sup>1</sup>Department of Materials Science and Engineering, University of California, Davis, CA 95616, USA<sup>2</sup>Department of Materials and Interfaces, Weizmann Institute of Science, Rehovot 76100, Israel<sup>3</sup>Max-Planck-Institut für Festkörperforschung, Heisenbergstraße 1, Stuttgart 70569, Germany

\*chmkim@ucdavis.edu; Igor.Lubomirsky@weizmann.ac.il

**Abstract**

The validity and limitations of two quantitative approaches for estimating the height of the potential barrier at grain boundaries,  $\Psi_{gb}$ , in polycrystalline ionic conductors are examined both theoretically and experimentally. The linear diffusion model recently proposed by Kim and Lubomirsky determines  $\Psi_{gb}$  from the value of the power exponent of the current ( $I_{gb}$ )-voltage ( $U_{gb}$ ) relationship at the grain boundary,  $d\ln(I_{gb})/d\ln(U_{gb})$ , while the conventional approach calculates  $\Psi_{gb}$  from the ratio of the grain boundary resistivity to the grain core resistivity. The results of our theoretical analysis demonstrate that both approaches should yield consistent values for  $\Psi_{gb}$  if the ionic current through the grain boundary is limited exclusively by space charge. While the value of  $\Psi_{gb}$  obtained by the power law procedure is relatively insensitive to other causes of current obstruction, e.g. current constriction and/or local structure disorder, the resistance ratio method, if not explicitly corrected for these additional limitations, results in a considerable overestimate of the grain boundary potential barrier. Hence, it is possible to distinguish between grain boundary resistance due to the presence of space charge and that due to additional sources by comparing the values of  $\Psi_{gb}$  determined using each of the two methods. Our theoretical analysis is confirmed experimentally with 3 mol% Gd-doped ceria with and without an additional source of current constriction across the grain boundary.

## 1 Introduction

Over the years, numerous studies have convincingly demonstrated that grain boundaries in solid electrolytes that conduct oxygen ions or protons impede ionic transport.<sup>1-5</sup> This is a significant problem for numerous applications ranging from fuel cells and lithium-ion batteries<sup>6</sup> to resistive switching memories<sup>7</sup>. Electric charge trapped at the grain boundary core has been implicated in the formation of a neighboring space charge region depleted of ions. This region may extend a distance of a few Debye lengths (screening lengths, Appendix 1) from the core center and depress the effective ionic conductivity of the ceramics by many orders of magnitude. The parameter that characterizes the degree of depletion and, thereby, the strength of the influence of the space charge on ionic transport, is the height of the potential barrier, namely the grain boundary potential,  $\Psi_{gb}$ . Therefore accurately estimating  $\Psi_{gb}$  is an essential and often critical<sup>8-10</sup> step in optimizing the ionic current in solid electrolytes. To date,  $\Psi_{gb}$  has been exclusively determined by what we will call the RR model, i.e. by calculating the ratio,  $r_{gb}$ , of the effective resistivity of a single grain boundary,  $\rho_{gb}$ , to that of the grain interior,  $\rho_{\infty}$ . At a given temperature, this ratio is given by<sup>11,12</sup> (also see Appendix 2 for details):

$$(1) \quad r_{gb} = \frac{\rho_{gb}}{\rho_{\infty}} = \frac{\exp(z\Psi_{gb}/V_{th})}{2(z\Psi_{gb}/V_{th})}$$

where  $V_{th} = q / k_B T$  is the thermal voltage and  $z$ ,  $q$ ,  $k_B$  and  $T$  denote ion charge number, elementary charge, Boltzmann constant, and absolute temperature, respectively (for practical examples see<sup>13,14</sup>). Since  $r_{gb}$  can be estimated from a single impedance spectrum,  $\Psi_{gb}$  can be readily determined by Eq. (1). For large values of  $r_{gb}$  (i.e.  $\frac{\Psi_{gb}}{V_{th}} > 4.5$ ), as is often the case with proton and oxygen conducting solid electrolytes, Eq. (1) can be simplified with accuracy better than 1% as:

$$(2) \quad \Psi_{gb} = V_{th} \cdot (a \cdot \ln(r_{gb}) + b)$$

where the constants  $a=1.176$ ,  $b=1.835$  are for  $z = 1$ , and  $a=0.566$ ,  $b=1.040$  for  $z = 2$ , respectively.

Recently, Kim and Lubomirsky<sup>15,16</sup> have described an alternative to the RR method of determining  $\Psi_{gb}$ . It uses a linear diffusion model to calculate the current across a grain boundary,  $I_{gb}$ , as a function of applied bias,  $U_{gb}$ . This model (termed the I-V model) was initially developed to provide an explanation for the power law relationship between  $I_{gb}$  and  $U_{gb}$  ( $I_{gb} \propto U_{gb}^{n_p}$ ) observed experimentally for various oxygen-ion and proton conducting solid electrolytes (e.g. acceptor-doped  $\text{CeO}_2$  and  $\text{BaZrO}_3$ <sup>15-17</sup>). While thermionic emission theory predicts that  $I_{gb}$  should increase exponentially with  $U_{gb}$  ( $I \propto e^{U_{gb}}$ )<sup>18-20</sup> and thus has difficulty in describing the power law behavior of ionic conductors<sup>10,11</sup>, the I-V model<sup>15,16</sup> accurately reproduces the observed power law relationship. In addition, and most importantly, it also predicts that for a given grain boundary, the product of the power  $n_p = d \ln I_{gb} / d \ln U_{gb}$  and  $T$  is given by:

$$(3) \quad (n_p - f_{KL}) \cdot T \approx \text{const}$$

where the “KL factor”,  $f_{KL} = 0.41 \pm 0.05$ , is a constant found from numerical simulations<sup>15,16</sup> for  $\Psi_{gb}/V_{th} < 12$ . The relation between  $\Psi_{gb}$  and  $n_p$  can be approximated as<sup>15,16</sup>:

$$(4) \quad \Psi_{gb}/V_{th} \approx n_p/f_{KL}.$$

This relationship allows for direct determination of  $\Psi_{gb}$  from the dependence  $I_{gb} \propto U_{gb}^{n_p}$  measured at a given temperature.

As will be demonstrated below, our numerical comparison of the RR and I-V methods shows that the values of  $\Psi_{gb}$  determined using either Eq. (1) or Eq. (4) are consistent with each other over a sufficiently wide range of  $U_{gb}$ , if and only if the current obstruction at the grain boundary is due solely to space charge. Since, in analyzing experimental data, Eq. (1) consistently gives higher values of  $\Psi_{gb}$  than Eq. (4), the present work was undertaken to provide an explanation of this discrepancy. We examine the limits of applicability of each method both for the case in which space charge is the only factor limiting ionic transport across the grain boundaries, and for the case when additional factors, e.g. current constriction by a second phase and/or local structural disorder, are present. Such additional factors have been discussed in the literature<sup>2</sup> but direct evidence from electrical experiments has not been available. Here we also present experimental verification of the numerical comparison.

## 2 Numerical comparison of the RR and I-V methods for determination of the grain boundary potential.

### 2.1 Comparison of the basic assumptions of the RR and I-V models

For completeness, a summary of the mathematical derivations of the RR and I-V methods of determining  $\Psi_{gb}$  is provided in Appendix 2. For both methods, the following conditions are assumed to hold: a) the charge trapped in the grain boundary core is the only source of current obstruction; b) the trapped charge is distributed over a thickness on the order of a few Debye lengths and it generates  $\Psi_{gb}$  larger than  $V_{th}$  by at least a factor of five. Consequently, the decay of the electric field is close to linear; c) all species follow a Boltzmann distribution, which also implies that the diffusivity and mobility are related to each other via the Nernst-Einstein equation. The RR method assumes that that space charge region has a thickness  $\delta_{sc} = (4\Psi_0/V_{th})^{1/2}L_D$ , with  $L_D$  being the Debye length for an acceptor-doped ionic conductor in which the defect concentrations follow a Mott-Schottky profile. The I-V model assumes for the sake of simplicity that the space charge in the grain boundary core has a Gaussian distribution Eq. (A10) described by two parameters:  $d$  is half the thickness of the grain boundary and  $a$  is a constant defining the total charge trapped in the grain boundary core. With these assumptions, solution of Poisson’s equation (Eq. (A9)) for the I-V model describes the distribution of electrical potential and electric

field in the vicinity of a grain boundary (Figure 1a) in dimensionless units (Appendix 1). The corresponding current- voltage relationship is shown in Figure 1b. In dimensionless units, the resistance of a grain interior is equal to 1. Therefore, on a log-log plot (Figure 1b), the I-V characteristic of a material without grain boundaries is represented by a straight line with slope 1 ( $I_{gb} \propto U_{gb}$  in dimensionless form is  $j = u_{gb}$ ; Appendix 1) passing through the point (1,1) (the dashed line  $x=y$  in Figure 1b). The difference in the approach of the RR and I-V methods can, on the basis of Figure 1b, be graphically illustrated as follows.  $r_{gb}$  can be understood as the difference between the ohmic current in the low voltage ohmic regime and the line describing the material in the absence of grain boundaries (the dashed line  $x=y$  in Figure 1b). The I-V model depends on the slope of the super-ohmic region (Figure 1b). However, since both models share the same basic assumptions, one may expect that when space charge at the grain boundary is the sole source of current obstruction, then, in principle, both methods should give the same results for the height of the grain boundary potential. This expectation is explored below.

## 2.2 Numerical comparison of RR and I-V methods for the case of current limited solely by space charge

To compare the RR and I-V methods when current is limited only by space charge, we have simulated the I-V curves of a grain boundary using Eq. (A9) for a number of values of  $d$  and  $a$ , similar to ref. <sup>15</sup>, from which  $n_p$  and, subsequently,  $\Psi_{gb}$  were determined. We have also estimated  $r_{gb}$  in the low voltage ohmic regime,  $u_{gb} = U_{gb}/V_{th} \ll 1$ . For this calculation, the thickness of the space charge region,  $\delta_{sc}$ , at the grain boundary was approximated to be similar to that typically used for semiconductor devices (Figure 1a and Ref. <sup>21</sup>). Then, from the potential distribution,  $u_{gb}$  at a given current  $j = I_{gb}/J_0$  was determined for the case of  $u_{gb} \ll 1$ . From the values of  $j$ ,  $u_{gb}$  and  $\delta_{sc}$ , the value of specific resistance of the grain boundary was calculated. We then used Eq. (2) to compute  $\Psi_{gb}$  as predicted by the RR model.

As expected, the RR and I-V methods result in consistent values of  $\Psi_{gb}$  (Figure 2) to within 5% for  $\Psi_{gb}/V_{th} < 10$ , which is relevant to the vast majority of cases of practical importance. At larger values of  $\Psi_{gb}$  both methods overestimate  $\Psi_{gb}$  by  $\leq 15\%$ , which is still satisfactory (though less practically important). These results reflect the fact that the RR method of determining  $\Psi_{gb}$  must be considered a subset of the I-V method because the latter considers the complete  $I_{gb} - U_{gb}$  curve, while the former compares the resistance in the low voltage ohmic region with that of the grain interior. In the ideal case of trapped charge independent of applied voltage and in the absence of sources of current obstruction other than space charge, both models are in very good ( $\leq 5\%$ ) agreement.

## 2.2 Numerical comparison of RR and I-V methods for the case of current obstruction in addition to space charge

As discussed above, the RR and I-V methods were originally derived with the assumption that ionic conductivity at grain boundaries is dictated solely by the resistance in the space-charge regions,  $R_{sc}$ . On the other hand, in an experimental setting, the voltage drop across a grain boundary,  $U_{gb} = I_{gb} \cdot R_{gb}$  (with  $R_{gb}$  being the grain boundary resistance) may result from multiple causes. In addition to the resistance produced by space charge,  $R_{sc}$ , it may include contributions,  $R_{ex}$ , such as constriction resistance due to existence of a secondary phase, imperfect contacts between the grains or suppression of ion diffusivity due to local lattice distortion. Moreover, it is difficult to distinguish experimentally between  $R_{ex}$  and  $R_{sc}$  even with AC impedance spectroscopy. In this regard, understanding the limits of the applicability of these methods is of both theoretical and practical importance. Below we examine, theoretically as well as experimentally, the sensitivity of the RR and I-V methods to additional sources of current obstruction. The difficulty of a comprehensive mathematical treatment leads us to consider a simplified semi-quantitative approach.

Let us assume, as a first approximation, that the Nernst-Einstein relationship linking the mobility and the diffusivity still holds notwithstanding the fact that the diffusion coefficient is a function of position. Then the equation for the electrical current Eq. (A7) must be modified as:

$$(5) \quad j = \left[ n_i^+(x) \cdot (-\phi') - \frac{\partial n_i^+(x)}{\partial x} \right] \cdot \frac{1}{\Theta(x)}$$

where  $\Theta(x)$  is a function that takes on the value 1 sufficiently far away from the grain boundary and reaches a certain limiting value  $> 1$  at the grain boundary core. Then Eq. (5) can be rewritten as:

$$(6) \quad j \cdot \Theta(x) = \left[ n_i^+(x) \cdot (-\phi') - \frac{\partial n_i^+(x)}{\partial x} \right]$$

Combining this equation with Eq.(A5) yields an equation that is similar to Eq. (A9):

$$(7) \quad \phi''(x) + [\phi'(x) + n_{gb}^+(x) - 1] \cdot \phi(x) + \frac{\partial n_{gb}^+(x)}{\partial x} - j \cdot \Theta(x) = 0$$

If we assume the presence of an insulating secondary phase in the grain boundary core, then the current density increases in its vicinity. This leads directly to Eq. (7) with the same requirements for  $\Theta(x)$ . Therefore, numerical solutions of Eq. (7) can give a qualitative description of the applicability of the RR and I-V methods for the case of  $R_{gb} > R_{sc}$ .

For the sake of simplicity, we have assumed that the current constriction as a function of position is given by:

$$(8) \quad \Theta(x) = 1 + \theta_{ex} \cdot \exp\left[-\left(\frac{x - x_{gb}}{l_{ex}}\right)^2\right]$$

where  $\theta_{ex}$  characterizes the degree of additional constriction and  $l_{ex}$  characterizes the distance at which the

extra constriction occurs. Obviously for  $|x - x_{gb}| \gg l_{ex}$   $\Theta(x) \rightarrow 1$ , irrespective of the value of  $\theta_{ex}$ . Then Eq. (7) becomes identical to Eq. (A9). For the case of zero current flow, current constriction no longer plays a role and  $\Psi_{gb}$  remains the same both with and without constriction.

We have calculated the I-V curves for:  $u_{gb} = U_{gb} / V_{th} < 80$ , for a number of combinations of  $\theta_{ex}$  and  $l_{ex}$ , and for four different charge distributions with:  $a = 12, 10, 8$  and  $6$  at  $d = 1$  (Figure 3). For each set of parameters,  $r_{gb}$  and  $n_p$  were determined, and from these, the values of  $\varphi_{gb} = \Psi_{gb} / V_{th}$  for both the RR and I-V models. The calculations lead to a number of interesting results, the most important being that with increasing current constriction, the I-V curve shifts to lower current values, but the shape of the curve changes very little. For values of  $\varphi_{gb} = \Psi_{gb} / V_{th} < 7$ , the decrease is small but detectable (Figure 3a and b) while for higher values of  $\varphi_{gb}$ , there is almost no change in  $n_p$ . However, since the RR method depends on the effective resistance of the grain boundary, the increase in resistance due to constriction leads to overestimation of  $\Psi_{gb}$  (Figure 3a). This overestimate becomes less pronounced with increase in the height of the model potential barrier,  $\Psi_{gb}$  (Figure 3b-d) i.e., as the fractional contribution of the space charge to the total grain boundary resistance increases.

From the results in Figure 3, we may conclude the following. Firstly, from the difference in  $\Psi_{gb}$  determined between the RR and I-V methods it is possible to estimate the contribution of  $R_{sc}$  to  $R_{gb}$ . Secondly, since in the large majority of practical cases  $\varphi_{gb} < 7$  ( $n_p < 3$ ), adding a secondary phase causes a small decrease in  $n_p$  but a considerable increase in  $r_{gb}$ . Therefore, if two compositionally identical samples have different  $r_{gb}$  values but similar values of  $n_p$ , then this can be taken as an indication of a significant source of grain boundary resistance in addition to space charge. To verify this hypothesis, we have investigated ionic transport in 3 mol% Gd-doped ceria intentionally contaminated with small amounts of Si.

### 3 Grain boundary potential in Si-contaminated 3 mol% Gd-doped ceria

Dense polycrystalline ceramics of 3 mol% Gd-doped ceria without and with Si impurities (3GDC and 3GDC-Si, respectively) were prepared as described in <sup>22</sup>. Si in ceria is known to segregate to the grain boundaries to form an insulating siliceous phase <sup>23,24</sup>, leading to current constriction across the grain boundary. Figure 4 exhibits the variation in Si-content across the grain boundaries in a 3GDC-Si ceramic, measured using an energy dispersive X-ray spectroscopy (EDS) line scan. The intensity of the Si X-ray emission increases sharply at/near the grain boundaries, confirming that Si in the sample indeed segregates to the grain boundary region. Consequently, on the basis of the preceding (Section 0),  $R_{gb}$  in 3GDC-Si would be expected to be larger than in a nominally pure 3GDC ceramic due to the additional source of current obstruction. On the other hand, the bulk resistance,  $R_{\infty}$ , would remain approximately unchanged because the amount of residual Si in the bulk should be minimal.

The Cole-Cole plots of the complex impedance of a 3GDC-Si ceramic measured as a function of  $U_{gb}$  at 350°C in ambient air (Figure 5) consist of two semicircular arcs in series. The arc appearing at higher frequencies (Figure 5 inset) corresponds to the bulk impedance and is insensitive to  $U_{gb}$ . On the other hand, the arc in the lower frequency region, corresponding to the grain boundary impedance is much larger and decreases with  $U_{gb}$ . Using the best-fit equivalent circuit comprising two (RW) circuits in series, where W is a constant phase element and the parenthesis indicates that R and W are connected in parallel, the resistance and capacitance of the bulk and grain boundary can be determined separately.

An Arrhenius plot of the bulk and the grain boundary conductivities ( $\sigma_{\infty}$  and  $\sigma_{gb}$  respectively) of 3GDC-Si measured at temperatures between 300 and 400 °C, is shown in Figure 6. For comparison, the corresponding conductivities of a nominally pure 3GDC sample are also included. Figure 6 demonstrates that  $\sigma_{gb}$  of the 3GDC ceramic is higher than that of 3GDC-Si by a factor of approximately 3 while  $\sigma_{\infty}$  of both samples superimpose, confirming that the grain interior is not affected by Si contamination. The nearly identical activation energies,  $E_a$ , for grain boundary conductivity,  $\sigma_{gb}$ , determined for the two samples - 1.13 and 1.18 eV- agree with earlier findings<sup>23,24</sup> that siliceous phase precipitates between the grain boundaries partially block contacts between them (Figure 4).

The  $I_{gb}-U_{gb}$  curves for 3GDC-Si are plotted on a log-log scale for temperatures between 598 and 673K (Figure 7a) and display a power-law behavior,  $I_{gb} \propto U_{gb}^{n_p}$ . The value of  $n_p$  is unity for  $U_{gb}/V_{th} < 1$  regardless of temperature, while it is larger than 1 for  $U_{gb}/V_{th} > 2$ , gradually decreasing with temperature from 2.14 to 1.92. A direct comparison between the  $I_{gb}-U_{gb}$  curves for 3GDC at 598K with and without Si is shown in Figure 7b, along with the values of  $n_p$  in the ohmic and super-ohmic regions. We note that Figure 7b is well consistent with the results of the simulation presented in Figure 3a: **(1)**  $I_{gb}-U_{gb}$  curves shift to lower current values due to the additional current constriction and yet the shape of the curve is approximately unchanged. **(2)** At a given temperature, the value of  $n_p$  determined from the slope in the super-ohmic region of the sample doped with Si is lower (2.14) than that of the sample without Si (2.32). Furthermore, in agreement with the simulations,  $\Psi_{gb}$  determined from the I-V model is  $\approx 10\%$  lower in the Si-contaminated sample than in the Si-free sample. At the same time,  $\Psi_{gb}$  for the Si-containing sample as determined by the RR model is higher than that of the Si-free sample (compare Figure 8 with Figure 3a).

It is obvious from Figure 8 that for 3GDC the values of  $\Psi_{gb}$  deduced from the RR analysis are much larger than those predicted by the I-V a difference which is qualitatively consistent with results previously reported for 1 mol% rare earth doped ceria<sup>15</sup>. Eq. (1) yields even higher values of  $\Psi_{gb}$  for 3GDC-Si due to the larger values of  $r_{gb}$  resulting from the current constriction at the grain boundary. Since the additional current

restriction  $R_{ex}$  has little influence on the value of  $n_p = d \ln I_{gb} / d \ln U_{gb}$ , the I-V model is much less sensitive to current constriction other than that due to space charge even when  $R_{ex}$  is large.

Specifically for the case of the Si-contaminated GDC sample considered here, an estimate of the value of  $\Psi_{gb}$  may be obtained from the activation energies  $E_a$  of  $\sigma_{\infty}$  and  $\sigma_{gb}$  shown in Figure 6. Since there is little difference in the values of the activation energy for grain boundary conductivity of samples both with and without Si contamination- 1.13 and 1.18 eV- we conclude that the part of the grain boundary resistance that is not related to space charge, i.e.  $R_{ex}$ , remains unchanged between 300 and 400°C. Therefore, in this temperature range

$$(9) \quad \frac{d(R_{ex} + R_{sc})}{dT} \approx \frac{dR_{sc}}{dT}$$

Moreover,  $\Psi_{gb}$  also does not change significantly in this temperature range (Figure 8). Under these conditions, differentiating Eq. (1) yields:

$$(10) \quad E_{a,gb} - E_{a,\infty} \approx \Psi_{gb} \cdot z - V_{th} \text{ where } E_a \equiv - \frac{d \ln \sigma}{d(1/V_{th})}$$

The data in Figure 6 give an estimate of  $\Psi_{gb} \approx 250$  mV. This is much closer to the values found using the linear diffusion model and much lower than those calculated using the RR model (Figure 8). Finally, the values of  $\rho_{gb}$  that would arise exclusively from space charge with the potential  $\Psi_{gb}$  determined by the I-V model for the nominally pure 3GDC as a function of temperature can be calculated using Eq. (1). They are shown in Figure 9 along with the impedance spectroscopy-deduced data for  $\rho_{gb}$ . The calculated values of  $\rho_{gb}$  are much lower than the measured values, demonstrating that space charge is not the only source of grain boundary resistance even in nominally pure 3GDC, but rather originates from a combination of sources.

Among these sources of “non-space charge related” resistance in polycrystalline materials may be included segregation of dopant atoms to the grain boundaries. For the multicomponent system, Gd-doped ceria, Gd segregation was confirmed for doping levels not less than 25 mol% Gd<sup>25</sup>. However, the samples used in the present study contain only 3 mol%. Therefore, the changes in the grain boundary potential barrier between GDC with and without Si, as observed and reported in the manuscript, must be due solely to the addition of Si. However, when appropriate, the grain size dependent segregation of impurities<sup>26,27</sup> should be taken into account during analysis of “non-space charge” related contributions to the grain boundary potential barrier. The linear diffusion method for distinguishing grain boundary resistance due to space charge provides a tool to investigate these effects.

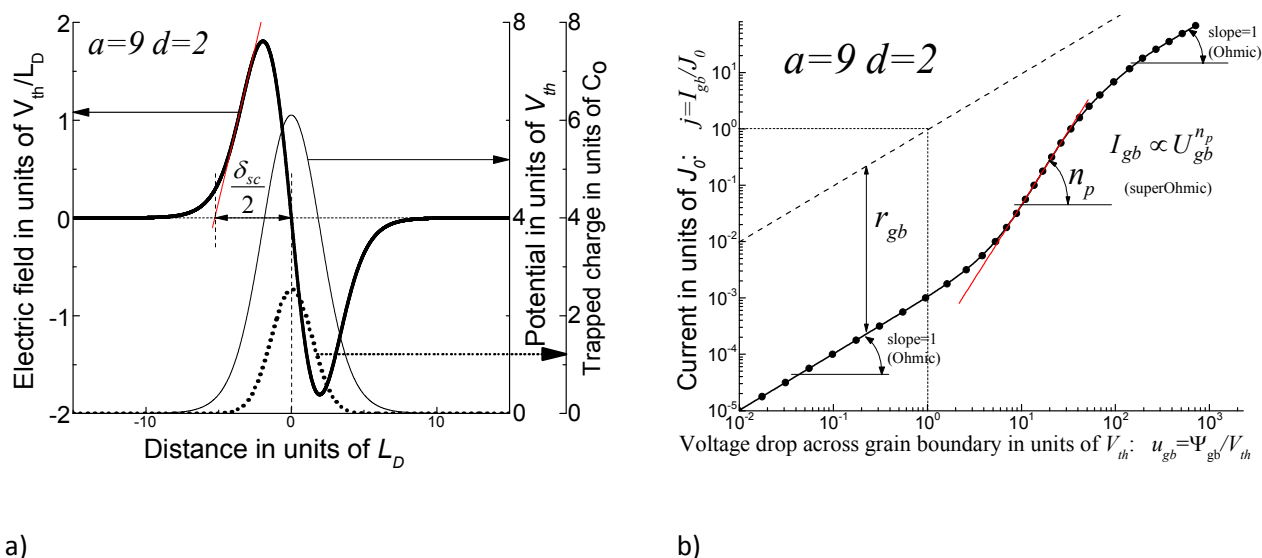
#### 4 Conclusion

We have examined both theoretically and experimentally the validity and limitations of the RR and I-V methods of calculating the height of the grain boundary potential barrier  $\Psi_{gb}$  in ionic conductors. The former method considers the regions of ohmic behavior of the  $I_{gb}-U_{gb}$  curve, in order to calculate the ratio of grain boundary resistivity to grain core resistivity and from there,  $\Psi_{gb}$ , while the latter determines  $\Psi_{gb}$  from the value of the power exponent,  $d \ln(I_{gb})/d \ln(U_{gb})$ , in the intermediate, super-ohmic region of the  $I_{gb}-U_{gb}$  curve:  $1 < U_{gb}/V_{th} < 80$ . The results of our numerical analysis demonstrate that if ionic current through a grain boundary is exclusively limited by space charge, the two models should yield similar results. In this case, the linear diffusion I-V model, which generates a complete  $I_{gb}-U_{gb}$  curve, rather than considering only its ohmic part, can be viewed as a generalization of the RR approach. This is consistent with the fact that both approaches share the same basic assumptions. However, if ion transport through the grain boundary is obstructed by causes other than space charge, e.g. current constriction or decrease in diffusivity due to local disorder, then a substantial difference in the values of  $\Psi_{gb}$  calculated by the two models is predicted. The additional obstruction does not significantly modify the value of  $\Psi_{gb}$  as determined by the I-V model, while a considerable overestimate of  $\Psi_{gb}$  is made by the resistivity ratio method. Therefore, by comparing the values of  $\Psi_{gb}$  determined by these two methods, it is possible to distinguish between grain boundary resistance originating from space charge and that arising from other sources, which recommends this procedure as a valuable tool for grain boundary engineering. Our theoretical analysis is confirmed experimentally by AC impedance spectroscopy measurements of a 3 mol% Gd doped ceria ceramic with and without intentionally introduced Si contamination. These data also indicate that even in nominally pure Gd-doped ceria, grain boundary resistance is larger than that resulting from space charge alone. This then constitutes the first direct experimental confirmation that even nominally pure solid electrolytes may have grain boundary resistance originating from sources other than space charge.

#### 5 Acknowledgements

S.K. and I.L. thank the US-Israel Binational Science Foundation (2012237) for funding this research. J.M. and I.L. express their deep appreciation to the Minerva foundation for supporting this research. I.L. wishes to acknowledge the assistance of the Nancy and Stephen Grand Research Center for Sensors and Security. The research is also made possible in part by the generosity of the Harold Perlman Family.

## 6 Figures



a)

b)

Figure 1. (a) Distribution of electrical potential and electric field simulated using Eq. (A9)<sup>15</sup> for a grain boundary with  $U_{gb}/V_{th}=0.02$  and with trapped charge characterized by a Gaussian distribution,  $a=9$  and  $d=2$  (Eq. (A10), Appendix 2.1).  $d$  is half the thickness of the grain boundary and  $a$  is a constant defining the total charge trapped in the grain boundary core. (b) Simulated current-voltage curve for this grain boundary illustrating three regimes, ohmic ( $I_{gb} \propto U_{gb}$ ) at  $u_{gb} = U_{gb}/V_{th} < 1$  and  $u_{gb} > 100$ , and super-ohmic ( $I_{gb} \propto U_{gb}^{n_p}$ ) at  $10 < u_{gb} < 80$ . The dashed straight line shows the I-V characteristic of a material without grain boundaries.  $\delta_{sc}$  is a thickness of the space charge layer used in RR model. Normalization constants are given in Appendix 1.

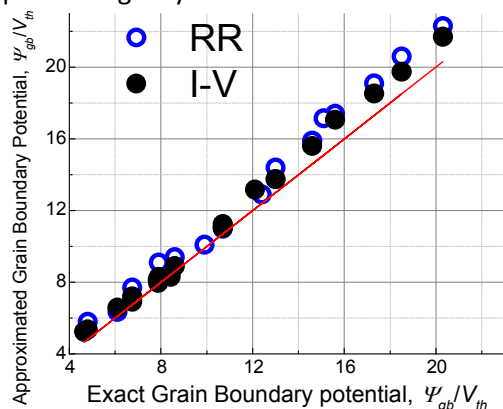


Figure 2. Comparison of the grain boundary potentials calculated using the RR and I-V methods when space charge is the only source of current restriction through the grain boundary.

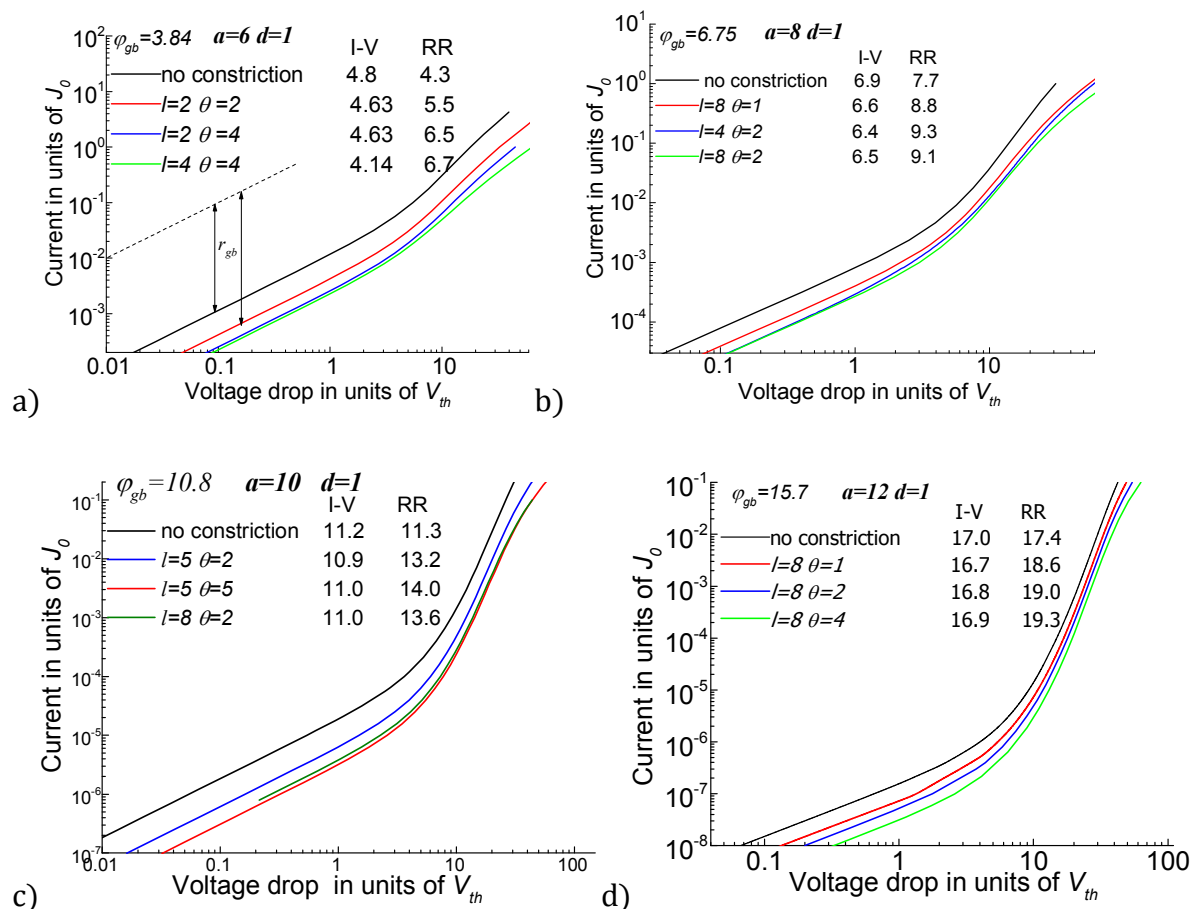


Figure 3. Simulated grain boundary I-V curves in the presence of space charge with and without additional current constriction (Eqs. (7) and (8)) due to partial blocking of the grain boundaries by an insulating layer. “No constriction” indicates space charge only. The dashed straight line in 3a shows the I-V characteristic of a bulk material without grain boundaries. The shift of the curves downward due to partial blocking of the grain boundaries by an insulating layer causes a significant change in  $r_{gb}$  but only slightly affects the slope of the super ohmic region.

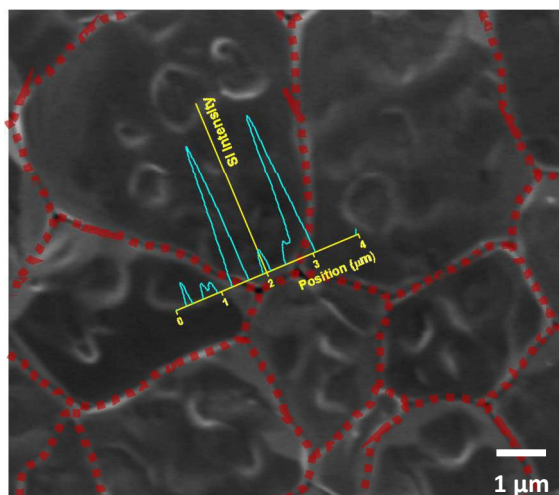


Figure 4. Variation in Si-content across the grain boundaries in a 3GDC-Si ceramic measured using an energy dispersive X-ray spectroscopy (EDS) line scan.

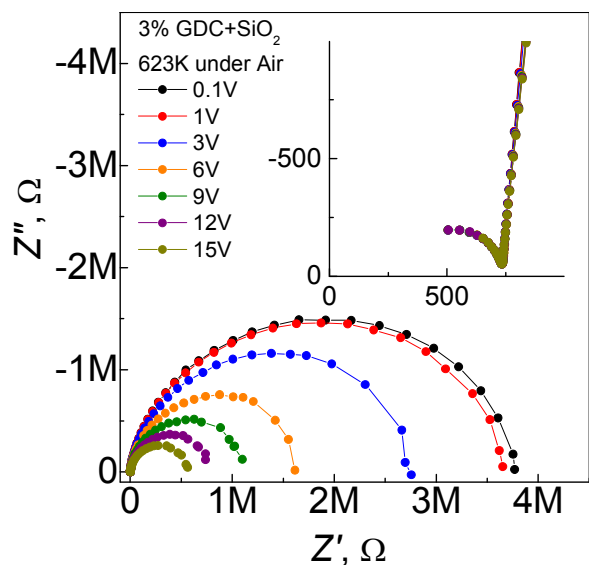


Figure 5. Cole-Cole plots of the complex impedance of a 3GDC-Si ceramic measured as a function of applied bias  $\approx U_{gb}^{15}$  at 350°C in air.

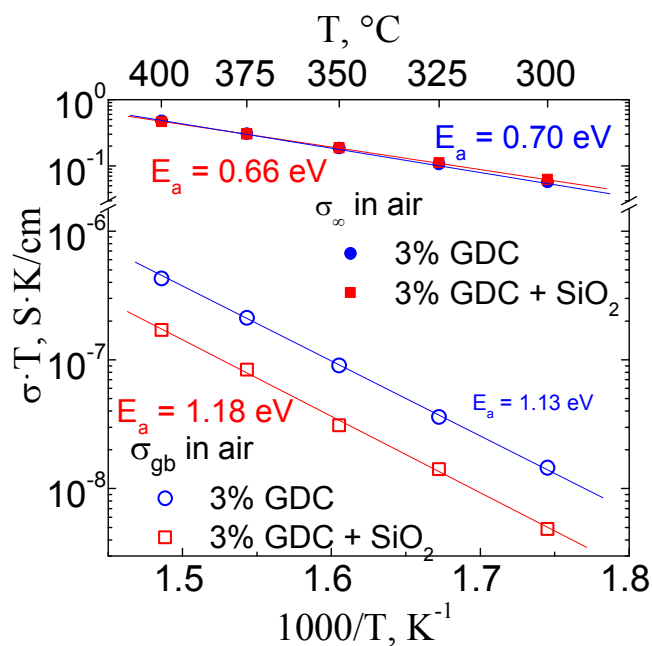


Figure 6. Arrhenius plot of the bulk and grain boundary conductivities ( $\sigma_{gb}$  and  $\sigma_{\infty}$ , respectively) of 3GDC-Si and 3GDC.

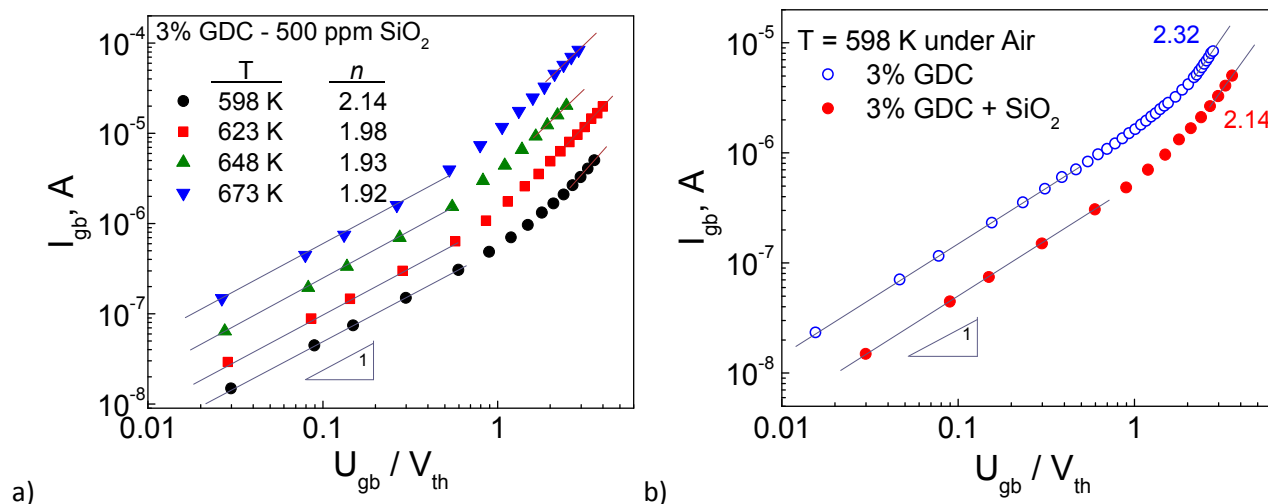


Figure 7. (a)  $I_{gb}$ - $U_{gb}$  curves of 3GDC-Si plotted on a log-log scale for temperatures between 325 and 402 °C. (b) Comparison between the  $I_{gb}$ - $U_{gb}$  curves at 325 °C for 3GDC both with and without Si.

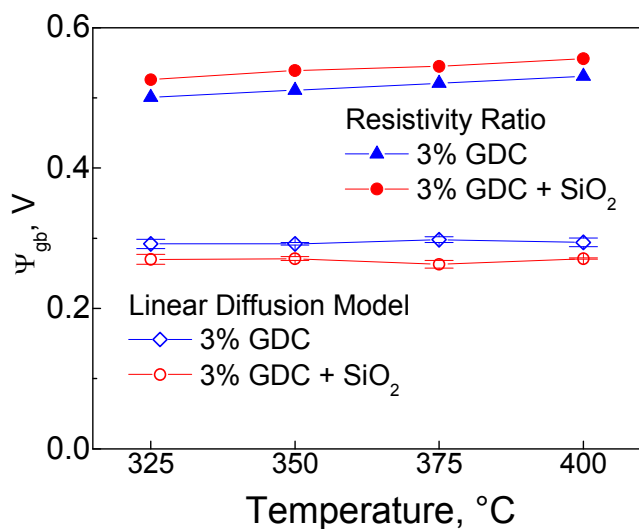


Figure 8. Values of  $\Psi_{gb}$ , estimated from the  $I_{gb}$ - $U_{gb}$  curves (Figure 7), using Eq. (1) (RR method) and Eq. (4) (I-V method) for samples of 3GDC both with and without Si. Presence of the siliceous phase reduces the values of  $\Psi_{gb}$  deduced by the I-V method and increases the values deduced by the RR method, as predicted in Figure 3a and b

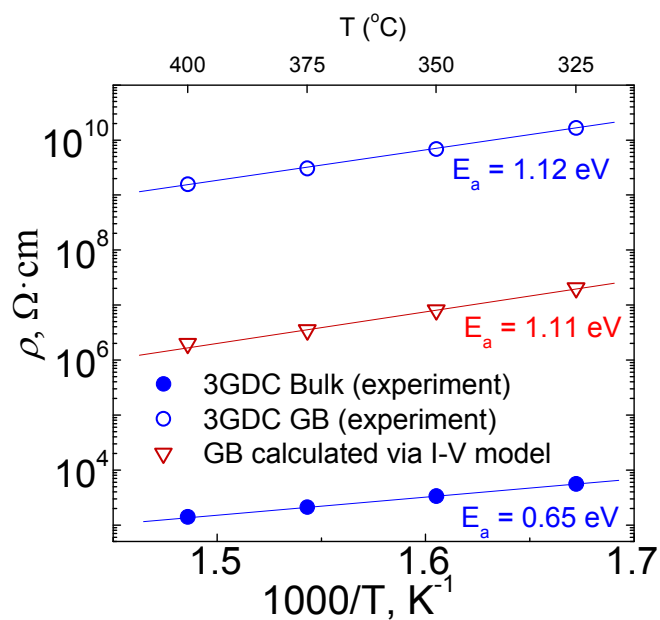


Figure 9. Grain boundary resistivity,  $\rho_{gb}$ , and bulk resistivity  $\rho_{\infty}$  of nominally pure 3GDC as determined by AC impedance spectroscopy and  $\rho_{gb}$  corresponding to the values of the grain boundary potential,  $\Psi_{gb}$ , calculated using the I-V model Eq. (3) with the data in Figure 7a.

## Appendix 1. Normalization units for the dimensionless equation of ion transport

Normalization units for the dimensionless equation of ion transport

(a) distance:  $x = X / L_D$ , where  $L_D = \sqrt{\frac{\varepsilon \cdot \varepsilon_0 \cdot k_B \cdot T}{q^2 \cdot C_i^+}}$  is Debye length;  $\varepsilon$  is a dielectric constant,  $\varepsilon_0$  is the

dielectric permittivity of vacuum

(b) potential:  $\varphi = \Psi / V_{th}$ , where  $V_{th} = k_B \cdot T / q$  is thermal voltage

(c) electric field:  $\phi = -\frac{E}{E_0} = -\frac{d\varphi}{dx}$ , where  $E_0 = V_{th} / L_D$

(d) concentration, in the units of charge per volume:  $n_i^+(x) = C_i^+(X) / C_i^+$ , where  $C_i^+(X)$  is the local concentration of mobile ions and  $C_i^+$  is the bulk concentration.

(e) current:  $j = I / I_0$  where  $J_0 = C_i^+ \cdot D \cdot q / L_D$ , where  $D$  is the ion diffusivity.

## Appendix 2. Derivation of RR and I-V model

We provide below a brief summary of the mathematical background for the RR and I-V methods. The two methods share the following assumptions: a) the charge trapped in the grain boundary core is the only source obstructing the current; b) the trapped charge is distributed over a thickness of the order of a few Debye lengths and it generates  $\Psi_{gb}$  larger than  $V_{th}$  by at least a factor of five. This assumption implies that the decay of the electric field is close to linear (Figure 1a); c) all the species follow a Boltzmann distribution, which also implies that the diffusivity and mobility are related to each other via the Nernst-Einstein equation.

### Appendix 2.1 Resistivity Ratio (RR) method of determining the grain boundary potential <sup>11</sup>.

At electrochemical equilibrium, the local concentration of a single dominant ionic charge carrier,  $C_i^+(x)$ , relative to that in the bulk of an ionic conductor,  $C_i^+$ , is, for dilute cases, given by the Boltzmann distribution:

$$(A1) \quad \frac{C_i^+(x)}{C_i^+} = \exp\left(-\frac{z_i \Psi_x}{V_{th}}\right)$$

where  $\Psi_x = \Psi(x) - \Psi_\infty$ ,  $z_i$  is the charge number of the ion and  $\Psi_\infty$  is the potential at a large distance from the grain boundary and  $x$  is a normalized spatial coordinate. The corresponding local resistivity,  $\rho(x)$ , relative to  $\rho_\infty$  is then

$$(A2) \quad \frac{\rho_i(x)}{\rho_{i\infty}} = \exp\left(\frac{z_i \Psi_x}{V_{th}}\right)$$

as  $\rho(x) \propto 1/C_i(x)$

According to the brick-layer model <sup>11</sup>, the space charge is concentrated in a narrow region. Therefore the electric field can be assumed to decay linearly as a function of distance from the grain boundary core and the effective resistivity of the space-charge layer,  $\rho_{sc}$ , can be approximated as:

$$(A3) \quad \rho_{sc} = \frac{1}{2\delta_{sc}} \int_0^{2\delta_{sc}} \rho(x) dx$$

where  $\delta_{sc}$  is the width of the space-charge region (Figure 1a) given as  $\delta_{sc} = (4\Psi_0/V_{th})^{1/2} L_D$ .  $L_D$  is the Debye length for an acceptor-doped ionic conductor in which the defect concentrations follow a Mott-Schottky profile. Combining Eqs. (A2) and (A3) yields  $\rho_{sc}$  relative to  $\rho_{\infty}$ ,

$$(A4) \quad r_{sc} = \frac{\rho_{sc}}{\rho_{\infty}} = \frac{\exp(z_i\Psi_{sc}/V_{th})}{2z_i\Psi_{sc}/V_{th}}$$

## Appendix 2.2 The I-V model of determination of the grain boundary potential

The I-V model is based on the interpretation of  $I_{gb} - U_{gb}$  relationships constructed from impedance spectra measured as a function of external bias at a fixed temperature. The model was developed by numerically solving the linear diffusion transport equation <sup>5,28</sup>. Below, we briefly provide justification for <sup>15,16</sup> this model. In dimensionless units (see Appendix 1), the space charge density is given by:

$$(A5) \quad \zeta(x) = n_i^+(x) - 1 + n_{gb}^+(x)$$

where  $n_i^+(x)$  and  $n_{gb}^+(x)$  are the concentrations of mobile ions and the trapped charge in the grain boundary core, respectively. Note that the capital symbol refers to the value in real units and lower-case symbol refers to the same value in dimensionless units. It should also be noted that the dopant concentration,  $c_d^-$ , is present in Eq. (A5) as  $c_d^- = C_d^-/C_i^+ = 1$ . For the space charge density distribution in Eq. (A5), the Poisson equation is:

$$(A6) \quad \phi''(x) = -\zeta(x) = 1 - n_i^+(x) - n_{gb}^+(x) \Rightarrow n_i^+(x) = 1 - \phi'(x) - n_{gb}^+(x)$$

Under the assumption that the Nernst-Einstein relation between ion mobility and diffusivity holds <sup>5</sup>, the electrical current can be described as the sum of electromigration (first term) and diffusion (second term) (i.e. the Nernst-Planck equation):

$$(A7) \quad j = n_i^+(x) \cdot (-\phi') - \frac{\partial n_i^+(x)}{\partial x}$$

Combining Eq. (A6) with Eqs. (A7), yields:

$$(A8) \quad j = [\phi''(x) + n_{gb}^+(x) - 1] \cdot \phi'(x) + \phi'''(x) + \frac{\partial n_{gb}^+(x)}{\partial x}$$

After setting  $-\phi'(x) = \phi$ , the equation with respect to electric field,  $\phi(x)$ , becomes <sup>15,16</sup>:

$$(A9) \quad \phi''(x) + [\phi'(x) + n_{gb}^+(x) - 1] \cdot \phi(x) + \frac{\partial n_{gb}^+(x)}{\partial x} - j = 0$$

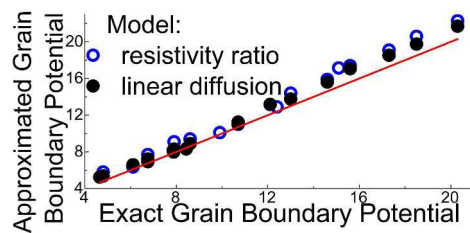
which is similar to that given in <sup>28</sup>. For simplicity, we describe the space charge in the grain boundary core, positioned at  $x_{gb}$ , by a Gaussian distribution:

$$(A10) \quad n_{gb}^+(x) = \frac{a}{d \cdot \sqrt{\pi}} \exp\left(-\frac{(x - x_{gb})^2}{d^2}\right)$$

where  $d$  is half the thickness of the grain boundary and  $a$  is a constant defining the total charge trapped in the grain boundary core  $Q_{gb} = C_i^+ \cdot L_D \cdot a$ . Similar to the RR method, the I-V model presented in refs. <sup>15,16</sup> is based on the assumption that **(i)** the space charge is the sole source of obstruction of ion transport through the grain boundaries; and **(ii)** the grain boundary core, where the trapped charge is concentrated, is much narrower than the space charge region, i.e.  $d \approx L_D$ . In addition, **(iii)** the model assumes that the charge in the grain boundary core is not altered by the external bias applied to the grain boundary at a given temperature. Under these conditions, numerical solution<sup>29</sup> of Eq. (A9) predicts that for voltage across the grain boundary  $U_{gb}/V_{th} < 2$ , the current is linearly related to the voltage  $I_{gb} \propto U_{gb}$  (i.e. ohmic) and for  $10 < U_{gb}/V_{th} < 80$ ,  $I_{gb} \propto U_{gb}^{n_p}$  (i.e. super-ohmic) (Figure 1b). In this region,  $10 < U_{gb}/V_{th} < 80$ , the following relations derived in refs. <sup>15,16</sup> hold:  $(n_p - f_{KL}) \cdot T \approx const$  and  $\Psi_{gb}/V_{th} \approx n_p/f_{KL}$ . For sufficiently large values of  $U_{gb}$  where  $U_{gb}/V_{th} > 100$ , the grain boundary becomes flooded by ions and the current again becomes proportional to the voltage:  $I_{gb} \propto U_{gb}$ , meaning that the grain boundary no longer affects the overall resistivity.

## 7 References

- 1 J. Fleig, S. Rodewald, and J. Maier, *J. Appl. Phys.* 2000, 87, 2372-2381.
- 2 X. Guo and J. Maier, *J. Electrochem. Soc.* 2001, 148, E121-E126.
- 3 S. Kim, J. Fleig, and J. Maier, *Phys Chem Chem Phys* 2003, 5, 2268-2273.
- 4 S. Kim and J. Maier, *J. Electrochem. Soc.* 2002, 149, J73-J83.
- 5 J. Maier, *Physical Chemistry of Ionic Materials: Ions and Electrons in Solids*, Wiley, 2004.
- 6 J. Maier, *Nat. Mater.* 2005, 4, 805-815.
- 7 R. Waser and M. Aono, *Nat. Mater.* 2007, 6, 833-840.
- 8 H. J. Avila-Paredes, K. Choi, C. T. Chen, and S. Kim, *J Mater Chem* 2009, 19, 4837-4842.
- 9 H. J. Avila-Paredes and S. Kim, *Sol. State Ionics* 2006, 177, 3075-3080.
- 10 F. Iguchi, C. T. Chen, H. Yugami, and S. Kim, *J Mater Chem* 2011, 21, 16517-16523.
- 11 S. Rodewald, J. Fleig, and J. Maier, *J. Am. Ceram. Soc.* 2001, 84, 521-530.
- 12 J. Fleig, *Sol. State Ionics* 2002, 150, 181-193.
- 13 C. Sanchez-Bautista, A. J. Dos Santos-Garcia, J. Pena-Martinez, and J. Canales-Vazquez, *Sol. State Ionics* 2010, 181, 1665-1673.
- 14 J. Fleig, B. Rahmati, S. Rodewald, and J. Maier, *J. Europ. Ceram. Soc.* 2010, 30, 215-220.
- 15 S. K. Kim, S. Khodorov, C. T. Chen, S. Kim, and I. Lubomirsky, *Phys Chem Chem Phys* 2013, 15, 8716-8721.
- 16 S. K. Kim, S. Khodorov, I. Lubomirsky, and S. Kim, *Phys Chem Chem Phys* 2014, 16, 14961-14968.
- 17 M. Shirpour, R. Merkle, and J. Maier, *Sol. State Ionics* 2012, 225, 304-307.
- 18 G. Blatter and F. Greuter, *Phys. Rev. B* 1986, 33, 3952-3966.
- 19 G. E. Pike and C. H. Seager, *J. Appl. Phys.* 1979, 50, 3414-3422.
- 20 R. Stratton, *Proc. Phys. Soc. B* 1956 69 513.
- 21 S. M. Sze, *Semiconductor Device Physics and Technology*, John Wiley & Sons, New York 1985.
- 22 R. Korobko, S. K. Kim, S. Kim, S. R. Cohen, E. Wachtel, and I. Lubomirsky, *Adv. Func. Mater.* 2013, 23, 6076-6081.
- 23 D. Perez-Coll, P. Nunez, and J. R. Frade, *J. Power Sources* 2011, 196, 8383-8390.
- 24 T. S. Zhang, J. Ma, S. H. Chan, P. Hing, and J. A. Kilner, *Solid State Sciences* 2004, 6, 565-572.
- 25 Z. P. Li, T. Mori, G. J. Auchterlonie, J. Zou, and J. Drennan, *Appl. Phys. Lett.* 2011, 98.
- 26 B. B. Straumal, A. A. Mazilkin, S. G. Protasova, S. V. Stakhanova, P. B. Straumal, M. F. Bulatov, G. Shutz, T. Tietze, E. Goering, and B. Baretzky, *Rev Adv Mater Sci* 2015, 41, 61-71.
- 27 S. G. Protasova, B. B. Straumal, A. A. Mazilkin, S. V. Stakhanova, P. B. Straumal, and B. Baretzky, *J. Mater. Sci.* 2014, 49, 4490-4498.
- 28 A. Leshem, E. Gonen, and I. Riess, *Nanotechnology* 2011, 22.
- 29 D. Kalaev and I. Riess, *Sol. State Ionics* 2012, 212 26.



Combining the linear diffusion and the resistivity ratio models, one can distinguish between the grain boundary resistance related to space charge from the resistance from other sources